Appl Phys B (2009) 97: 339–350
DOI 10.1007/s00340-009-3740-4

Applied Physics B
Lasers and Optics

Spectroscopy and lasing of cryogenically cooled Yb, Na:CaF_2

A. Pugžlys · G. Andriukaitis · D. Sidorov · A. Irshad · A. Baltuška · W.J. Lai · P.B. Phua · L. Su · J. Xu · H. Li · R. Li · S. Ališauskas · A. Marcinkevičius · M.E. Fermann · L. Giniūnas · R. Danielius

Received: 21 April 2009 / Revised version: 5 August 2009 / Published online: 22 September 2009

Abstract Absorption, photoluminescence and cw-lasing properties of a novel Na^+-codoped Yb^{3+}:CaF_2 laser crystal are investigated in the temperature range from 10 K to 290 K. Cryogenic cooling leads to the disappearance of the ground-state absorption in the spectral region above 1000 nm and a substantial increase of emission and absorption cross-sections. A particular advantage of the Yb^{3+}, Na^+-codoped CaF_2 crystal lies in the possibility of a direct pumping in the vicinity of the zero phonon line while nearly perfectly avoiding an overlap with the stimulated emission. Further advantages of the low-temperature operation are demonstrated by achieving a close to the theoretical limit slope efficiency of 92% in a cw-laser operation with an output coupler of 28%. By seeding stretched pulses from a femtosecond Yb fiber oscillator into a cryogenically cooled DPSS Yb^{3+}, Na^+:CaF_2 regenerative amplifier, we obtain >3-mJ pulses at a 1-kHz repetition rate with a spectral bandwidth exceeding 12 nm. The pulses are compressed with a single grating compressor to 173 fs as verified by SHG FROG. Shaping of the spectral amplitude of the seed and active control of the higher-order phase is shown to be crucial for obtaining sub-200-fs pulses at multi-mJ energies.

PACS 42.55.Rz · 42.55.Xi · 42.60.Da · 42.60.Lh · 42.65.Re

A. Pugžlys (✉) · G. Andriukaitis · D. Sidorov · A. Irshad · A. Baltuška · S. Ališauskas
Photonics Institute, Vienna University of Technology, Gusshausstrasse 27-387, 1040, Vienna, Austria
e-mail: pugzlys@tuwien.ac.at

S. Ališauskas
Laser Research Center, Vilnius University, Saulėtekio av. 10, 10223 Vilnius, Lithuania

W.J. Lai · P.B. Phua
Nanyang Technological University, 21 Nanyang Link, Singapore 637371, Singapore

L. Su · J. Xu · H. Li
Key Laboratory of Transparent and Opto-functional Inorganic Materials, Shanghai Institute of Ceramics, Chinese Academy of Sciences, 1295# DingXi Rd., Shanghai, 200050, People's Republic of China

R. Li
Shanghai Institute of Optics and Fine Mechanics, Chinese Academy of Sciences, 390# Qinghe Rd., Shanghai, 201800, People's Republic of China

A. Marcinkevičius · M.E. Fermann
IMRA America Inc., 1044 Woodridge Ave., Ann Arbor, MI 48105, USA

L. Giniūnas · R. Danielius
Light Conversion Ltd., P/O Box 1485, Saulėtekio av. 10, 10223 Vilnius, Lithuania

1 Introduction

Rapidly developing areas of femtosecond laser technology, metrology and high-field physics demand high-average-power femtosecond laser systems operating at multi-kHz repetition rates and delivering multi-mJ pulses which can be used either as direct high-field sources for extreme nonlinear optics [1] or, alternatively, as pump sources for optical parametric chirped pulse amplifiers [2]. The average power versus pulse energy scaling in ultrafast laser amplifiers poses a well known difficulty [3]. For example, Ti:sapphire femtosecond amplifiers operating at kHz repetition rates rarely exceed the energy level of a few milli-Joules and the average power of several Watts because of the thermal management and/or optical damage problems.

In comparison with Ti:sapphire, the Yb^{3+} materials offer a very low quantum defect and can be pumped directly by laser diodes, making it very easy to attain high average powers in Yb^{3+} oscillators [4–8]. Pursuing the goal of Yb-based high-energy pulse amplification, numerous regenerative amplifiers based on Yb^{3+}-doped active medium were designed. A few prominent examples, typifying different trends of development, include a Ti:sapphire-laser-pumped Yb^{3+}-doped glass regenerative chirped-pulse amplifier operating at a 10 Hz repetition rate, [9]; a Ti:sapphire or directly diode pumped Yb:KGW ps/fs regenerative amplifiers [10]; a femtosecond thin-disk Yb:KYW regenerative amplifier [11]; cw-diode-pumped Yb^{3+}:$SrY_4(SiO_4)_3O$ regenerative amplifier producing 70-μJ pulses at 1 kHz [12]; a pulsed-laser-diode pumped multi-mJ Yb^{3+}:CaF_2 regenerative laser amplifier operating at 1 Hz repetition rate [13] and others. Furthermore, very recently the first pulsed-laser-diode pumped Yb^{3+}:CaF_2 multipass chirped pulse amplifier capable of reaching terawatt peak power has been demonstrated [14].

Although Yb crystals generally exhibit very long fluorescence lifetimes, frequently longer than 1 ms, obtaining high gain is very challenging because their emission cross-section is 20–30 times lower than that of Nd and Ti:sapphire [15]. Very high laser saturation and pump saturation intensities (e.g. for Yb:KGW and Yb:YAG ∼ 10 kW/cm^2 and ∼30 kW/cm^2, respectively) require an exceptionally tight diameter of the pump [16] and cavity modes. The tight mode size becomes a problem for mJ-class chirped-pulse amplifiers, especially for Yb:YAG and Yb:KGW/KYW, the materials most established to date for regenerative and multi-pass amplification of femtosecond pulses. This is caused by the high linear and nonlinear refractive indices; a narrow gain linewidth (Yb:YAG); and a high Raman susceptibility (KGW/KYW), limiting the scaling of the output pulse energy [10].

Yb-doped fluorides represent an interesting alternative because of their transparency in a wide wavelength region from the VUV to the IR; low linear and nonlinear refractive indices and low nonradiative relaxation between adjacent energy levels. Among different fluoride hosts, CaF_2—one of the first host materials since the early 1960s [17, 18] and the very first host material to be used with direct diode pumping at cryogenic temperatures [19]—has one of the lowest phonon frequencies (328 cm^{-1}) and a high thermal conductivity (around 10 Wm^{-1} K^{-1} at room temperature and 39 Wm^{-1} K^{-1} at 83 K [20]). Recently, a modified host, Yb^{3+}, Na^+:CaF_2 was introduced, where Na^+ has been suggested to act as a charge compensator in CaF_2 [21, 22]. As was shown in [21], codoping with Na^+ leads to significant modifications of the spectroscopic properties, especially to an increase of the radiative lifetime.

In recent years cryogenic cooling was applied in a number of lasers systems based on Yb-doped materials. T.-Y. Fan and coworkers have developed a 300-W cw-pumped cryogenically cooled Yb:YAG laser [23]. A 24-W diode-pumped micro-Joule level picosecond multipass amplifier with a liquid nitrogen (LN2)-cooled Yb:YAG crystal has been reported [24]. Realization of an LN2-cooled Yb^{3+}:YLF-doped regenerative amplifier, delivering tens of mJ at a repetition rate of 20 Hz was reported by Yamakawa and coworkers [25], followed by the demonstration of a Yb:KYW regenerative amplifier operating at 10 Hz repetition rate [26]. Such interest in the cryogenically cooled Yb amplifiers [27, 28] is determined by the following key advantages expected at low temperatures: (a) the disappearance of the ground-state absorption above 1000 nm, i.e. an effective transition to a four-level scheme; (b) an increase of the emission cross-section, i.e. higher single-pass gain and a decreased saturation fluence; (c) an increase of thermal conductivity, leading to an improved dissipation of parasitic heat, a lower thermal lens, an increased thermal fracture threshold and a decreased thermally induced birefringence; (d) a greater radiative lifetime; (e) a decreased pump saturation intensity. Stronger emission and absorption at low temperatures, in principle, allow one to lower the Yb concentration in comparison with the room temperature conditions, thus providing room for further increase of the crystal fracture threshold [29].

In this paper, we examine the optical properties of the new Yb, Na:CaF_2 host at room and cryogenic temperatures and compare it with the previously reported low-temperature studies of the sodium-free Yb:CaF_2 [30, 31]. In addition, the cw-lasing of Yb, Na:CaF_2 is characterized and the performance of a cryogenically cooled Yb, Na:CaF_2 regenerative amplifier (CRA) is presented.

The paper is organized as follows: the methods of Yb, Na:CaF_2 crystal characterization and experimental details are given in Sect. 2. The results of the investigation of the spectroscopic properties and lasing of Yb, Na:CaF_2 combined with the performance analysis of the CRA are presented in Sect. 3, followed by the conclusions, which are formulated in Sect. 4.

2 Materials and experiments

2.1 Crystals

The Yb-doped and Yb, Na-codoped CaF_2 single crystals were grown by the Temperature Gradient Technique (TGT) method. The raw materials were YbF_3 (99.99%), CaF_2 (99.99%), NaF (99%), and PbF_2 (99%). The melting temperature of the raw materials is ∼1380°C. In all cases, 0.5 wt% PbF_2 was used as an oxygen scavenger. For the growth of Yb, Na-codoped CaF_2 crystal samples, NaF was added in an excessive amount. After weighing the ratios of

the input materials, the fractions were thoroughly mixed, pressed into blocks, and loaded into a graphite crucible, which in the cylindrical section measures 78 mm in diameter. Prior to launching the growth procedure, the entire furnace is evacuated to the pressure of 10^{-3} Pa. At first, the furnace temperature is maintained at 673 K for 10–20 h to expel water from the raw materials and the furnace chamber.

Two variations of the growth technique for Yb, Na-codoped samples were tested: one using an inert gas buffer atmosphere, and one under vacuum. In the first case, the chamber was filled with a buffer atmosphere of a highly purified Ar gas at the pressure of 1.1 atm before starting the actual crystal growth. This method was used to produce 2%Yb:CaF_2 and 2%Yb0.38%Na:CaF_2 crystals. Due to a high volatility of NaF at the melting point of CaF_2 and a low segregation coefficient, the actual concentration of Na in CaF_2 crystal corresponds only to an ∼10% of the dopant concentration in the introduced raw material (NaF). Conversely, the Yb concentration in the grown crystals corresponds rather well to the proportion of YbF_3 in the introduced raw material.

For the crystals grown under the vacuum conditions, the retained concentration of Na is substantially lower as compared with the case of the Ar buffer gas and was estimated to be less than 0.1%. For both methods after the raw materials were melted, the crystal growth was controlled by lowering the temperature at the rate of 3 K/h. The crystals were then cooled to room temperature. The concentrations of Yb and Na in the crystals were measured by an Inductively Coupled Plasma Atomic Emission Spectrometry (ICP–AES) analysis. In this work we compare Yb, Na-codoped CaF_2 specimens grown according to the two different sets of conditions, described above, with a CaF_2 doped with Yb only. For the clarity of reference, we introduce the following labeling of the different CaF_2 materials tested in this study: **A** for a 2%Yb-doped crystal; **B** for a 2%Yb, <0.1%Na codoped material; and **C** for a 2%Yb, 0.38%Na codoping.

2.2 Spectroscopy

For the measurement of absorption and luminescence spectra of Yb:CaF_2 and Yb, Na:CaF_2 at various temperatures, AR-coated slabs, prepared for each crystal type and measuring 4 mm in length and 1.2 mm in height, were sandwiched between two parts of a copper heatsink using a layer of indium foil. The crystal assembly was then mounted inside a continuous flow He cryostat (Oxford Research, model MicrostatHe). The absorption spectra were recorded using the tungsten halogen lamp LS1 and USB2000 spectrometer from Ocean Optics. The luminescence spectra were recorded and cross-checked by the USB2000 spectrometer and an optical spectrum analyzer (AQ-6315A, Yokogawa). The excitation source was a single-emitter 978-nm laser diode operating either in the cw- or a pulsed mode, respectively, for the measurement of luminescence spectra and luminescence decay times. Luminescence decay kinetics was measured with a Si photo-detector (DET36A/M, Thorlabs) and a digital 300-MHz oscilloscope (TDS3034B, Tektronix), using 200-μs-long excitation pulses from the single-emitter laser diode. To ascertain the influence of reabsorption on the depopulation dynamics, the luminescence decay measurement was repeated on the tip of a sharp needle-like splinter of crystal **B**.

2.3 Lasing

The lasing properties of Yb, Na:CaF_2 crystal (crystal **B**) at various temperatures were tested in a short (30-cm-long) cavity cw-laser consisting of two high reflectors (R = 99.885%) (Fig. 1). The crystal was end-pumped from one side with a 40-W 19-emitter diode bar from DILAS. A set of microlenses (Light Conversion, Ltd.) attached to the diode module was used to image the light from each individual emitter onto a single spot located approximately 50 mm in front of the diode bar assembly (point F in Fig. 1). The pump spot F is re-imaged into the CaF_2 crystal using a 2f–2f configuration with a spherical R = −70 mm mirror CM. A ∅3-mm hole in the center of the concave pump mirror served pass through the intracavity laser beam while ensuring that nearly the full available pump power reaches the crystal. The minimal pump losses through the central hole are explained by a specially chosen configuration of the micro-optics, ensuring that the hole on the mirror coincides with a low-pump-intensity region. The combined

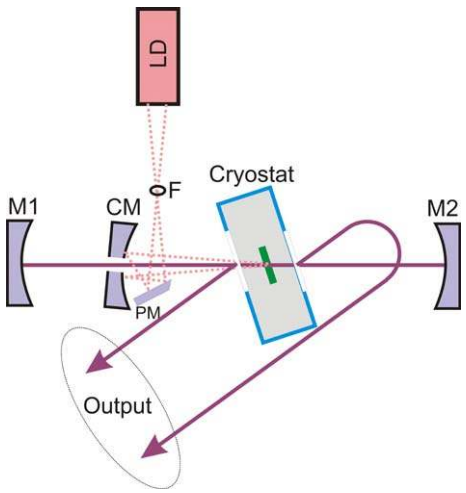

Fig. 1 Schematic of the test cavity. LD—laser-diode bar, M1, M2—concave cavity mirrors with R = −200 mm, CM—2f-to-2f imaging mirror with R = −70 mm, PM—sharp edge mirror, F—the spot where light from all emitters of the LD is collected. Arrows indicate 8 reflections at a near-normal incidence (4 reflections per single pass) off the cryostat windows

reflections off the uncoated windows of the cryostat provide an effective ∼28% output coupler for the intracavity energy. The emission wavelength of the laser pump diode was set at 977 nm where, as will be explained in Sect. 3.1, the crystal absorption practically stayed invariant with temperature.

2.4 Small signal gain

The small signal single-pass gain in the Yb, Na:CaF_2 crystal (crystal **B**) was measured in a pumping configuration nearly identical to the one in the cryogenically cooled regenerative amplifier, which is explained in Sect. 2.5, using an end pump from both optical faces of the CaF_2 slab with a total incident pump power of about 60 W. A tunable seed beam for this measurement synthesized from the output of a femtosecond Yb fiber laser by selecting a narrowband frequency component with a slit placed in the Fourier plane of the pulse stretcher used for regenerative amplification and described in Sect. 3.4. The seed beam was chopped by an optomechanical chopper (Thorlabs) and detected, after a single-pass amplification, with a Lock-in amplifier (SRS00545, Stanford Research Systems).

2.5 Regenerative amplifier

The layout of the CRA cavity is presented in Fig. 2. An AR-coated slab of crystal **B** with the length of ∼4 mm and the height of 1.2 mm is sandwiched using an optical contact between two plates of artificial diamond (Diamond Materials GmbH), which are soldered with indium onto a copper heatsink. The crystal assembly is mounted inside a cryogenic chamber and cooled to the temperature of 110 K with a closed-loop refrigerator (CryoTiger). The crystal is pumped in a double-side, double-pass configuration depicted in the lower panel of Fig. 2 with two 60-W diode laser bars (Jenoptik Laserdiode GmbH) supplied with sets of microoptics (Light Conversion, Ltd.). The double-pass pumping is possible because of the isotropic nature of CaF_2 and is realized by employing a quarter-lambda wave plate and a thin-film polarizer which, respectively, perform a 90° polarization rotation and rejection of the unabsorbed returning pump light. Because the overall estimated quantum defect of our system is <5%, the crystal temperature increases very modestly to ∼140 K under the full combined pump power of both diodes. The pump-induced thermal lens in the Yb^{3+}, Na^{+}:CaF_2 crystal is estimated from a comparison between the results of a numerical intracavity beam tracing and the beam profile measurements at various positions in the cavity. The thermal lens under cw-lasing conditions and 50 W of incident pump power is $f \approx -500$ mm. The temperature of the diode bars was set to optimize the spectral overlap between the diode emission spectrum and the blue side of the zero phonon line (ZPL) of the laser crystal. The dichroic mirror DM in the cavity (Fig. 2) was installed to suppress parasitic lasing around 990 nm corresponding to the strongest emission line of Yb^{3+}.

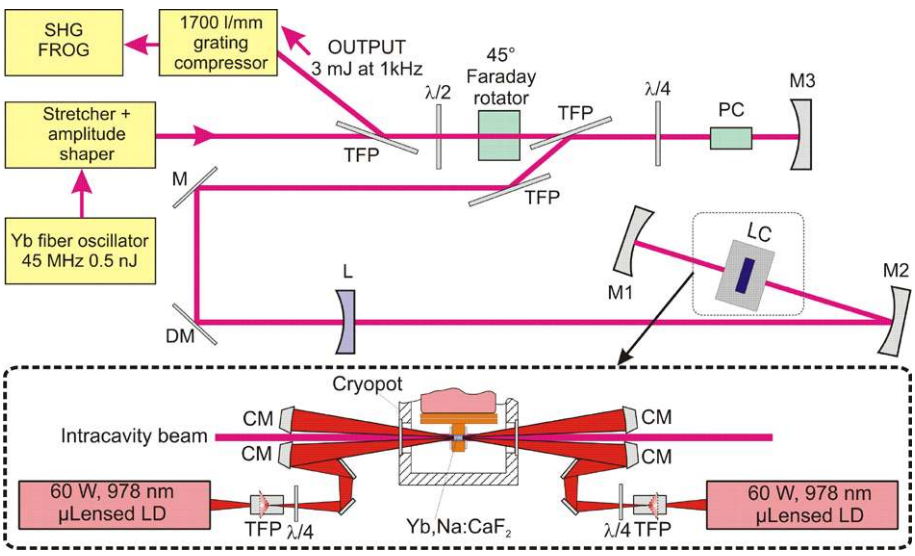

Fig. 2 Schematic of cryogenically cooled Yb^{3+}, Na^{+}:CaF_2 RA. M1, M2 and M3 are concave mirrors with ROC −300 mm, −500 mm and −2500 mm respectively, LC—cryogenically cooled laser crystal chamber, L—negative lens, f = −400 mm, DM—dichroic mirror, M—folding mirror, TFP—thin-film polarizers, PC—Pockels cell, λ/2 and λ/4—half- and quarter-waveplates, LD—60-W 978-nm laser-diode bars. The separation distances between M1–crystal–M2–L–M3 for the generation of 3-mJ pulses (see text for details) are 365, −350, −235, and 1050 mm, respectively. The repetition rate of the RA cavity is ∼75 MHz. Lower panel shows the schematics of the double-pass pumping

3 Results

3.1 Spectroscopy

Spectroscopic properties of the Na-free Yb:CaF_2 at cryogenic and room temperatures at various dopant concentrations were examined in detail previously [30, 31]. Hexameric clusters of Yb^{3+} ions were identified as lasing centers of Yb:CaF_2 at the concentrations of Yb^{3+} above 0.1 at.% [31]. Here we concentrate on the comparison of the optical properties of Yb:CaF_2 crystals with and without the Na^+ codoping. The overview of the measured absorption spectra for the crystals **A**, **B**, and **C** cooled to the temperature of 10 K is presented in Fig. 3a. Here we are following the transition assignment for Yb:CaF_2 crystals given in detail in [30, 31] and marked on a simplified Yb^{3+} energy level diagram is shown in Fig. 3b. The influence of Na codoping is examined on both the absorption and emission spectra. A progressive decrease of the overall absorption and a modification of the absorption spectrum is observed with the growth of the Na concentration. In particular, at higher Na concentrations, band **1** at 919 nm (labeled as a $1 \rightarrow 7$ transition in [30]) is substantially suppressed, whereas a shoulder at 922 nm emerges as peak **2**, for which we are unable to offer a clear assignment at this time. Furthermore, at increased Na concentrations, a sharp peak **3** at 962.5 nm (attributed to the absorption of cubic O_h sites [31]) becomes significantly more pronounced, and a shoulder at 976 nm (**4**) appears on the blue side of the ZPL while the ZPL intensity at 978 nm (band **5**) exhibits a substantial drop. Although the origin of band **4** is unknown, its appearance substantially broadens absorption in the vicinity of the ZPL. On the one hand, the presence of this extra band gives Yb, Na:CaF_2 an advantage with respect to other broadband Yb crystalline hosts by relaxing the wavelength tolerance for diode pumping. In practical terms, this provides a unique opportunity to pump Yb, Na:CaF_2 into the vicinity of the ZPL even at cryogenic temperatures using conventional laser-diode stacks (typically of a 3–4 nm spectral FWHM) without Bragg grating wavelength stabilization. On the other hand, as it will be discussed in Sect. 3.2, band **4** permits a more efficient pumping of the laser crystal while avoiding the region of overlap between the absorption and emission. In the latter region, the energy scheme effectively corresponds to a two-level system, which results in the loss of available population inversion. The importance of band **4** is highlighted in the insets to Fig. 3a and b: in the case of the Na codoped Yb:CaF_2 the overlap of the 4-nm FWHM laser-diode spectrum with the absorption spectrum on the blue side of the ZPL is substantial (Fig. 3a, inset) whereas the overlap with the luminescence spectrum (Fig. 3b, inset) is negligible. Noteworthy, for the assumed diode spectrum, the overlap with the emission band **5′** in the case of a sodium-free crystal is nearly the same as in the case of the crystals with sodium. However the overlap with the absorption spectrum is significantly poorer in comparison with the Na-codoped crystals. By choosing a more red-shifted pump wavelength, the overlap with the absorption spectrum in Yb:CaF_2 can be substantially improved, but this would occur at the expense of the inversion loss through stimulated emission. Therefore, with respect to the available absorption bandwidth and the opportunity parasitic emission losses, the Na-codoped crystals at cryogenic temperatures are clearly superior to Yb:CaF_2.

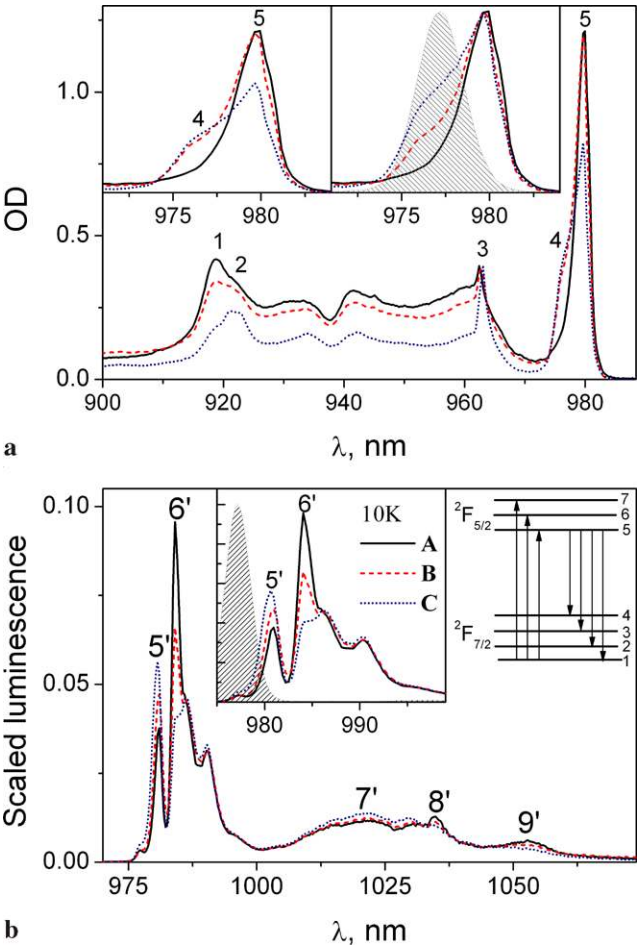

Fig. 3 (**a**) Absorption spectra of crystals **A** (*solid line*), **B** (*dashed line*) and **C** (*dotted line*) measured at the temperature of 10 K. The insets zoom into the spectral region around the ZPL and show directly measured (*left*) and normalized (*right*) data. The numbers from 1 to 5 indicate the spectral regions sensitive to Na codoping (for details see text). (**b**) Emission spectra of crystals **A** (*solid line*), **B** (*dashed line*) and **C** (*dotted line*) measured at the temperature of 10 K and normalized according to their respective areas. The inset zooms into the spectral region of 975–1000 nm. Numbers from 5′ to 9′ indicate spectral regions sensitive to Na codoping (see text for details). A simplified energy level diagram of Yb^{3+} is shown in the top right corner. The hatched contours in the insets of panels (**a**) and (**b**) represent the spectrum of the laser-diode (LD) bar

Emission spectra measured at 10 K and scaled to their integral area as $I_{em}(\lambda)/\int I_{em}(\lambda)\,d\lambda$ are presented in Fig. 3b.

Modification of emission properties of Yb:CaF_2 by Na codoping is mainly pronounced in the spectral range of 975–990 nm and is manifested by an increase of the ZPL (band **5′**) intensity. This increase can be explained by the fact that the absorption and, consequently, the re-absorption become lower. There is also a notable decrease of the emission in the vicinity of 985 nm (band **6′** of an unknown origin [31]). A weak contribution on the blue side of ZPL (with the maximum at ∼976 nm) is not related to the emission properties and is caused by scattered light from the excitation laser diode. Emission on the long wavelength side is modified in a far less pronounced way: with the increase of the Na content, the emission intensity is slightly increased in the spectral region of 1010–1030 nm (corresponding to band **7′**, which is assigned to vibronic transitions [30]). At the same time the relative intensities decrease in bands **8′** and **9′**, which corresponding to the transitions $5 \rightarrow 3$ and $5 \rightarrow 4$ [30]. In addition, a minor blue shift of transitions **7′**, **8′** and **9′** is observed. This causes a modest narrowing of the emission spectrum with the increase of the Na concentration.

The modification of both the absorption and emission spectra as a function of Na concentration is similar to the dependence observed by Ito et al. [30] for an increase of the Yb^{3+} doping concentration in CaF_2 from 0.5% to 30%. The change of the spectral properties of emission was explained in terms of lowering of the crystal field for higher dopant concentrations and by the formation of various types of Yb clusters. The lowering of the crystal field with an increase of the Na concentration in an Yb, Na:CaF_2 crystal at room temperature was also reported by Su et al. [21].

Further we concentrate on the temperature-dependent optical properties of the crystal **B**, which was subsequently used in the studies of the lasing and laser amplification properties. Regardless of the Na^+ codoping, all tested Yb-doped CaF_2 crystals have shown a significant increase of absorption at cryogenic temperatures (Fig. 4), especially in the vicinity of the ZPL, and a progressive disappearance of the ground-state absorption (GSA) on the red side of the ZPL as a function of temperature decrease. Moving from low to high temperatures, the influence of the Na codoping for the absorption linewidth broadening of the blue side of the ZPL remains considerable up to the temperature of ∼170 K. For higher temperatures, thermal broadening overshadows the feature and the 976 nm absorption in the crystals **A** and **B** equalizes.

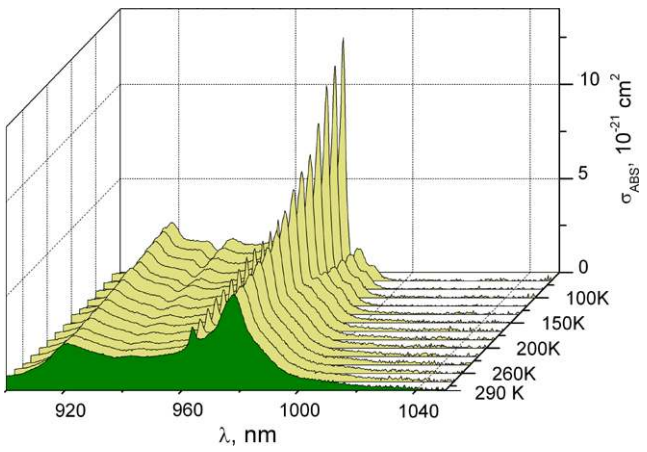

Fig. 4 Absorption cross-sections of the crystal **B** in the temperature range 80–290 K

From the measured absorption and luminescence spectra, the emission cross-sections of crystal **B** were recovered by combining the reciprocity relationship and the Füchtbauer-Ladenburg method [32]. Before the calculation of the emission cross-sections, the emission spectra were first corrected for the re-absorption by using a relationship:

$$I_f(\lambda) \propto I_f^m(\lambda)\left[\frac{\ln T(\lambda_f) + \ln T(\lambda_{\text{pump}})}{1 - T(\lambda_f)T(\lambda_{\text{pump}})}\right]. \quad (1)$$

$I_f^m(\lambda)$ and $I_f(\lambda)$ in (1) represent the measured and corrected emission spectra while $T(\lambda_f)$ and $T(\lambda_{\text{pump}})$ are the crystal transmission at the emission and excitation wavelengths, respectively. Note that in view of the narrowness of the ZPL, the accuracy of the correction for re-absorption in its vicinity can be limited by the spectral resolution of the USB2000 spectrometer. Because of the unknown luminescence quantum yield, the radiative lifetime of the crystal was estimated by scaling the emission cross-sections, calculated using two methods, in the region of spectral overlap between the absorption and emission [32]. Furthermore, the measured luminescence lifetime at different temperatures (Fig. 5a) allows an estimation of the luminescence quantum yield. The luminescence lifetime was measured in a bulk crystal and on a sharp edge of a fraction of the crystal (Sect. 2.2). In a bulk crystal, the luminescence lifetime is influenced by the re-absorption and, as the result it shortens with the temperature decrease because of the disappearance of GSA. Conversely, in the case of the measurement on the sharp crystal edge, where the re-absorption is insignificant, the luminescence lifetime stays nearly invariant with temperature down to 80 K and amounts to ∼1.7 ms. The obtained radiative lifetimes reveal the decrease of the luminescence quantum yield by approximately 15%—from ∼0.69 to ∼0.59—in the process of raising the temperature of the sample from 80 K to room temperature (Fig. 5b).

The absorption and emission cross-sections at the temperatures of 110, 170 and 290 K, corresponding, respectively, to the lowest and the highest crystal temperatures achievable with the closed-loop refrigerator (Cryotiger), and to room temperature are given in Fig. 6. With the temperature increase, the absorption cross-section is strongly reduced. Nevertheless, it stays practically invariant in the vicinity of 976 nm, which is due to the broadening in the

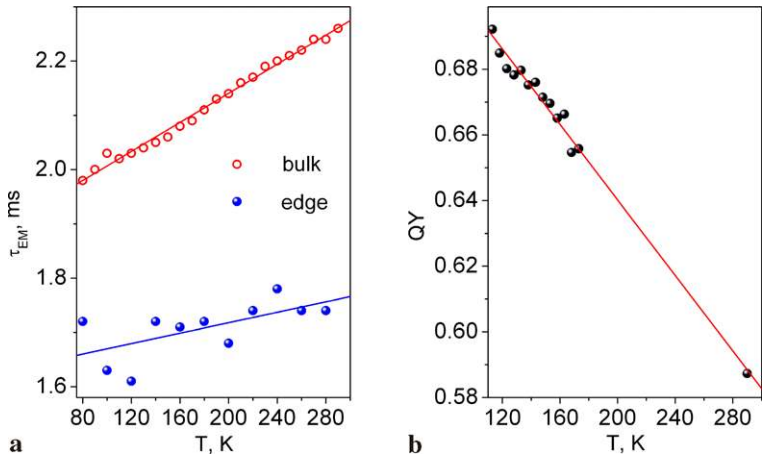

Fig. 5 (**a**) Dependence of the emission lifetime of crystal **B** as measured in a 4-mm thick slab (*open circles*) and on the sharp edge of the crystal fraction (*filled circles*). *Solid lines* are guides to the eye. (**b**) Dependence of the emission quantum yield of crystal **B** on the temperature

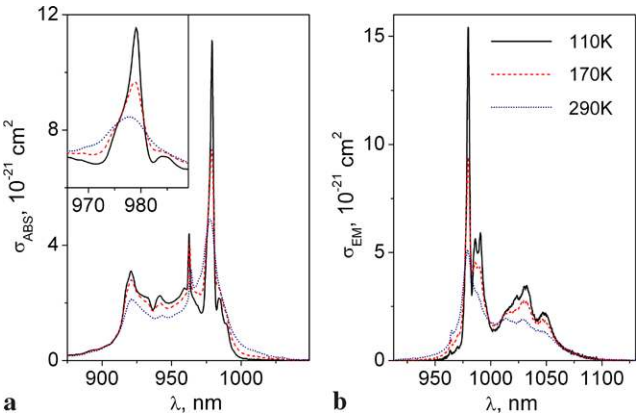

Fig. 6 Absorption (**a**) and emission (**b**) cross-sections of crystal **B** at temperatures of 110 K (*solid line*), 170 K (*dashed line*) and 290 K (*dotted line*). In the *inset* to panel (**a**), the absorption cross-section is zoomed in the vicinity of the ZPL

vicinity of ZPL addressed above. This indicates that a practically constant pump absorption level can be maintained for a broad temperature range for the pump wavelength of 976 nm. In contrast with the absorption properties, the changes of the emission cross-section as a function of the crystal temperature are considerably more pronounced: at higher temperatures a substantial decrease of the cross-section is observed between 1020 and 1050 nm—the primary region of interest for lasing and pulse amplification.

The calculated absorption and emission cross-sections allow for the estimation of the gain cross-sections $\sigma_{\text{gain}} = \beta\sigma_{\text{em}} - (1-\beta)\sigma_{\text{abs}}$. In Fig. 7a, the gain cross-sections calculated for the fraction of the excited-state population $\beta = n_{\text{excited}}/n_{\text{tot}} = 0.5$ are given for the temperatures of 110, 170 and 290 K. The β value of 0.5 was chosen taking into account the value of the excited-state population obtained in the small signal gain measurements (cf. Sect. 3.2). For $\beta = 1$, the gain cross-section is equivalent to the emission cross-section and thus can be used as an indication of the maximum gain cross-section achievable with the crystal at an infinitely high pump rate. Calculated gain cross-sections reveal that at low temperatures, unlike in Yb:KGW and even in another fluoride host, YLF [25, 33], the gain cross-section of Yb, Na:CaF_2 remains remarkably smooth and broadband, making it a promising host for cryogenic regenerative amplification of sub-200-fs pulses. Furthermore, a substantial decrease of gain cross-section with the increase of the temperature (Fig. 7b) underscores the advantage of cryogenic cooling for robust laser amplification.

3.2 Small signal gain

In Fig. 8a, the small signal gain coefficient of crystal **B**, cooled to 110 K, measured at the seed wavelength of 1030 nm, is presented as a function of absorbed pump power. The absorbed pump power was calculated by subtracting the power transmitted through the crystal from the incident laser-diode output power. Measurements of the crystal temperature have revealed that with an increase of the absorbed pump power to 70 W the temperature of the crystal rises to 140 K. For the given pump spot size and excited crystal volume, corresponding to the experimental conditions in the CRA (Sect. 3.4), we measured the highest single-pass small signal gain of 1.33, obtained at 40 W of absorbed pump power. The crystal temperature in the pumped region was 130 K as independently confirmed by identifying the known temperature-dependent features of the emission spectrum. With a further increase of the absorbed pump power, the gain coefficient starts to decline. This behavior is related to the temperature- and current-dependent red shift of the laser-diode emission spectrum. At the current corresponding to the absorbed powers above 40 W, the spectrum of the diode starts to overlap substantially with the ZPL, which, because of an increased probability of stimulated emission causes "forced" depopulation of the excited state and leads to a decreased population inversion. The effect of the temperature-related red shift can be offset by lowering

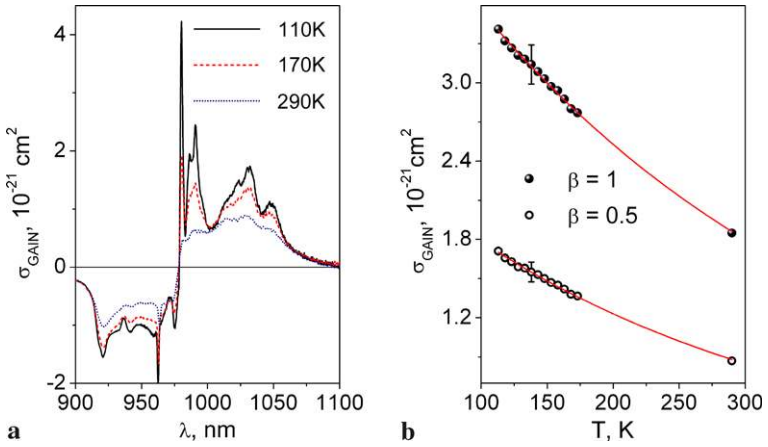

Fig. 7 (**a**) Gain cross-section of crystal **B** at temperatures of 110 K (*solid line*), 170 K (*dashed line*) and 290 K (*dotted line*). (**b**) Dependence of gain cross-section for the crystal **B** at 1030 nm on temperature for two fractions of the excited-state population: $\beta = 0.5$ (*open circles*) and $\beta = 1$ (*filled circles*); the *lines* are guides to the eye

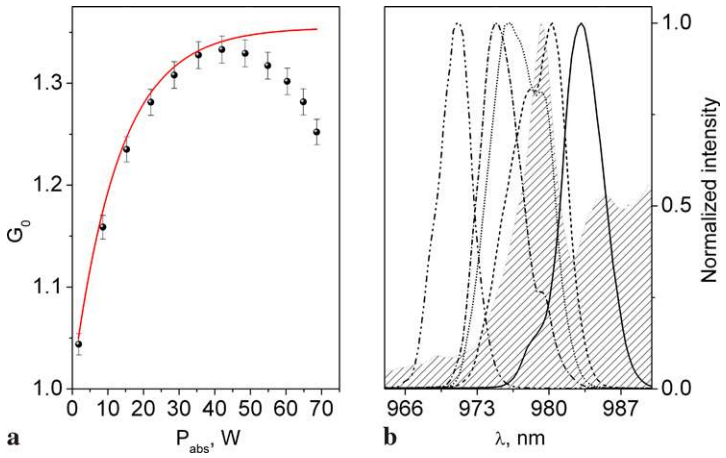

Fig. 8 (**a**) Small signal gain at 1030 nm measured at 110 K for crystal **B** as a function of absorbed pump power (*dots with error bars*). The *solid line* represents a calculated small signal gain in the absence of stimulated emission (for details see text). (**b**) Current-dependent shift of the laser-diode spectrum transmitted through the crystal at the current of 10, 35, 40, 45 and 60 A (*from left to right*). Emission spectrum of the crystal **B** at temperature 130 K is shown by a hatched contour

Table 1 Values of the parameters used for the calculation of small signal gain at 1030 nm

L, cm	σ_{em}[a], 10^{-21} cm^2	n_{tot}, cm^{-3}	τ_{rad}[a], ms	ν_p, Hz	V, cm^3	η	η_Q	η_S	η_B
0.4	3.2	4.91×10^{20}	2.5	3.1×10^{14}	2.8×10^{-4}	0.59	0.687	0.95	0.9

[a]σ_{em} and τ_{rad} are given at 130 K

the water temperature in the diode chiller, so that the emission wavelength at high currents still avoids an overlap with the stimulated emission region. However, lowering the water temperature below the dew point was not attempted as it endangers the diodes. Therefore, selecting more blue-shifted diodes would have allowed achieving a higher gain for the same experimental conditions.

The measured small signal gain data were fitted using the formalism described in [34, 35] and involving absorption saturation due to the ground-state depletion:

$$G_0 = \exp\left[L\sigma_{em}n_{tot}\left(\frac{\frac{\eta P_{abs}\tau_{rad}}{h\nu_p V n_{tot}}}{\frac{\eta P_{abs}\tau_{rad}}{h\nu_p V n_{tot}} + 1}\right)\right]. \quad (2)$$

L in (2) is the crystal length, σ_{em} is the emission cross-section, n_{tot} is the concentration of Yb^{3+} in the crystal, P_{abs} is the absorbed pump power, τ_{rad} is the radiative lifetime, $h\nu_p$ is the pump photon energy, V is the excited volume and $\eta = \eta_Q\eta_S\eta_B$ is the efficiency factor with η_Q, η_S and η_B being the quantum efficiency, Stokes factor, and overlap factor between the seed mode and gain volume, respectively. η_B was considered a fitting parameter because the gain distribution and its dynamic change cannot be fully accounted for under our experimental conditions. The values of the parameters are given in the Table 1.

As shown in Fig. 8a, the calculated curve follows the measured data up to 35 W of the absorbed pump power. The discrepancies start when diode spectrum begins to overlap with the ZPL. According to Fig. 8b, the pump light, transmitted through the crystal, is substantially enhanced in the overlap region with the ZPL of the emission spectrum, which reveals a forced depopulation of the excited state and

a decreased gain. In Fig. 9a, the logarithm of the small signal gain measured at the absorbed pump power of 35 W is plotted together with the emission cross-section spectrum measured at 130 K. The perfect agreement between the two sets of data reveals the good precision and consistence of both the evaluation of emission cross-section and the measurements of the small signal gain. Furthermore, we recall that $G_0 = \exp(\sigma_{em} \Delta n L)$ with Δn being the available population inversion. Under the conditions of our cryogenic temperatures, assuming an initially empty lower lasing state for the transition around 1030 nm, Δn corresponds to the concentration of excited Yb^{3+} ions in the upper lasing level. Therefore, the obtained data allow one to estimate the population inversion in absolute terms. This is a very important result because, as is evident from (2), the population inversion depends on a number of such critical parameters as η, V, and τ_{rad} which are difficult to evaluate precisely. From the calculated σ_{em} and measured G_0 we have estimated the value of Δn to be 2.26×10^{20} cm^{-3}. Taking into account the total Yb^{3+} concentration of 4.91×10^{20} cm^{-3} in the 2%Yb:CaF_2 crystal, this value of Δn corresponds to $\beta = 0.46$ in the case of a 35-W absorbed pump power.

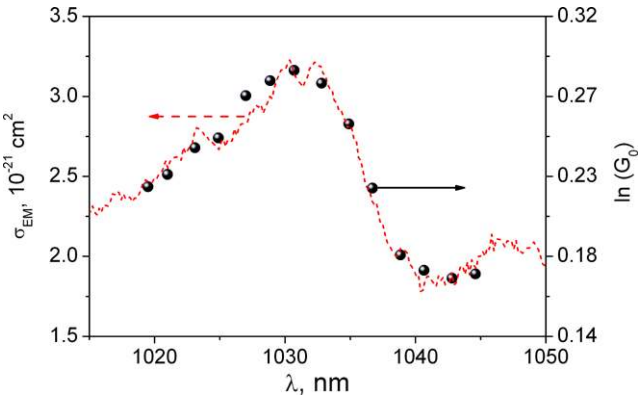

Fig. 9 Emission cross-section (*dotted line*) measured at the temperature of 130 K and the logarithm of the measured small signal gain in the case of a 35-W absorbed pump power

3.3 Lasing

The cw-lasing properties of crystal **B** were tested in a short cavity configured as described in Sect. 2.3. The laser emission was centered at 1030 nm. Figure 10 depicts the slope efficiencies and threshold pump powers obtained at various temperatures in the case of an effective 28% outcoupling, determined by 8 reflections off the uncoated cryostat windows. The wavelength of the pump diode was set at 976 nm, such that the crystal absorption practically stayed invariant with temperature (see Sect. 3.2). The slope efficiency [35, 36] of 92%, which is close to the theoretical limit, was obtained in the temperature range of 80–100 K. This range also corresponds to the lowest threshold pump power. With a further increase of the crystal temperature, the slope efficiency gradually drops down while the threshold pump power rises. Finally, for the available pump power range, no lasing was obtained above 210 K because the optical cavity losses and the losses due to GSA are too high.

3.4 Performance of Yb, Na:CaF_2 regenerative amplifier

Based on the spectroscopic and small signal gain studies, presented above, we have designed a cryogenically cooled Yb, Na:CaF_2 regenerative amplifier, schematically sketched in Fig. 2. The output of the CRA exhibits an excellent spatial profile and a rather high slope efficiency. As shown in Fig. 11, the beam profile is virtually ideally Gaussian in both the vertical and horizontal cross-sections with the M^2 of ∼1.05 measured in the seeded (picosecond) operation regime.

In the cw-mode, the 2-m-long CRA cavity delivers more than 14 W output at the incident pump level of ∼60 W. In the initial experiments, 3-mJ 12-ns-long pulses at a 1-kHz repetition rate were generated in the Q-switched regime, whereas in the ps operation mode the seed pulses were amplified to a 2-mJ level (Fig. 12). The incident pump power on the crystal was 60 W and 36 W, respectively. Further amplification

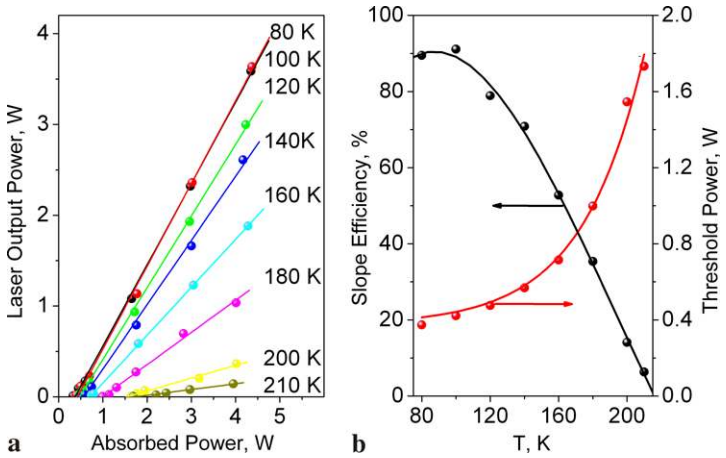

Fig. 10 (**a**) Slope efficiencies measured at 1030 nm at various temperatures (indicated in the panel) in the case of an effective 28% out-coupling. (**b**) Dependence of the slope efficiency and lasing threshold on the temperature

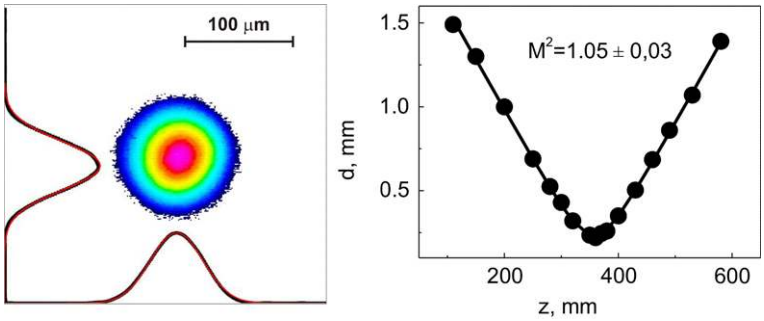

Fig. 11 *Left*: profile of the 1-mJ 1-kHz output beam at the focus of an f = 300-mm lens measured in the case of picosecond operation; *black* and *red solid curves* show, respectively, experimentally measured vertical and horizontal beam profile cross-sections and corresponding Gaussian fits; *Right*: M^2 measurement; *dots*—experimental data, *line*—a fit corresponding to M^2 of 1.05

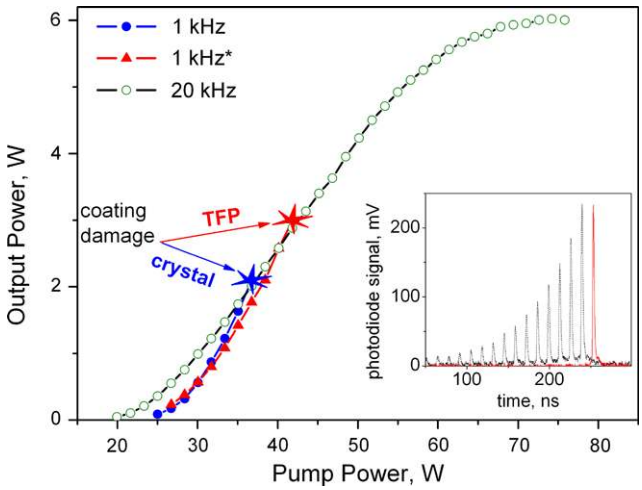

Fig. 12 Dependence of the output power on the pump power in the case of picosecond operation at the repetition rate of 1 kHz in the case of two CRA cavity configurations (see text for details) and at 20 kHz. The insert shows an oscillogram of the pulse train (*dashed black line*) and of the selected pulse (*red solid line*) taken in the case of the generation of 3 mJ pulses

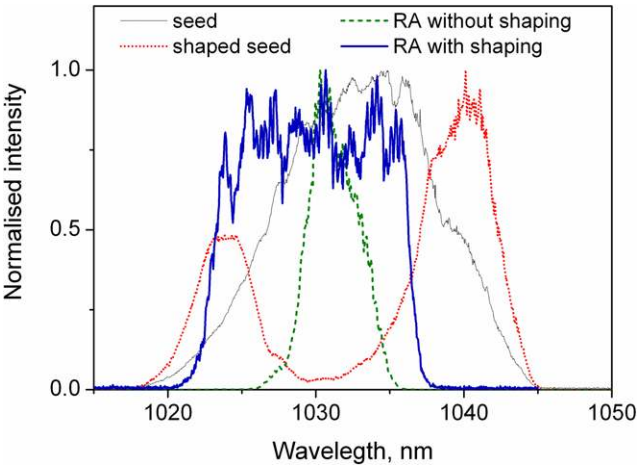

Fig. 13 Spectra of the seed laser before (*thin dotted line*) and after (*thick dotted line*) shaping, and resulting spectra of the CRA output without (*dashed line*) and with (*solid line*) the amplitude shaper installed

in the case of the 1-kHz repetition rate was prevented by the optical damage of AR coatings of the crystal. At a 20-kHz repetition rate, ps pulses were amplified to a 300-μJ level, corresponding to the average extracted power of 6 W. It is important to note that the average power saturation at 20 kHz is partly due to a decreased pump absorption efficiency caused, as discussed in Sect. 3.1 by the red shift of the pump diode wavelength at higher currents, and partly due to a small beam spot size on the Yb:CaF_2 crystal (∅300 μm at the $1/e^2$ level).

To test the feasibility of the amplification to higher pulse energies, an adjustment of the cavity configuration was made mainly by increasing the distance between mirror M1 and the crystal and adjusting the position of the intracavity lens L. This increased the mode size on the crystal surfaces and allowed the generation of >5 mJ nanosecond pulses in the Q-switched regime and the amplification of picosecond pulses to 3 mJ at a 1-kHz repetition rate (Fig. 12). However, this modification has also resulted in a decreased spot size on the thin-film polarizers (TFP) leading to an optical damage of the TFP coating. It is important to notice that neither the pulse train saturation (inset in the Fig. 12) nor a bi-stable behavior (bifurcations) of the pulse train are present in the 3-mJ 1-kHz output despite an ∼1.7-ms effective storage time of the laser crystal. This reveals a possibility of further scaling of the amplified pulse energy by improving the quality of the dielectric coatings and/or adopting a Brewster-angle-cut CaF_2 crystal.

In the picosecond operation, the CRA was seeded by a stretched to 240 ps output of a femtosecond Yb fiber laser operating at the repetition rate of 45 MHz. The fiber laser generates 25-nm FWHM broad spectrum with the maximum at 1034 nm. The positive dispersion stretcher is based on a

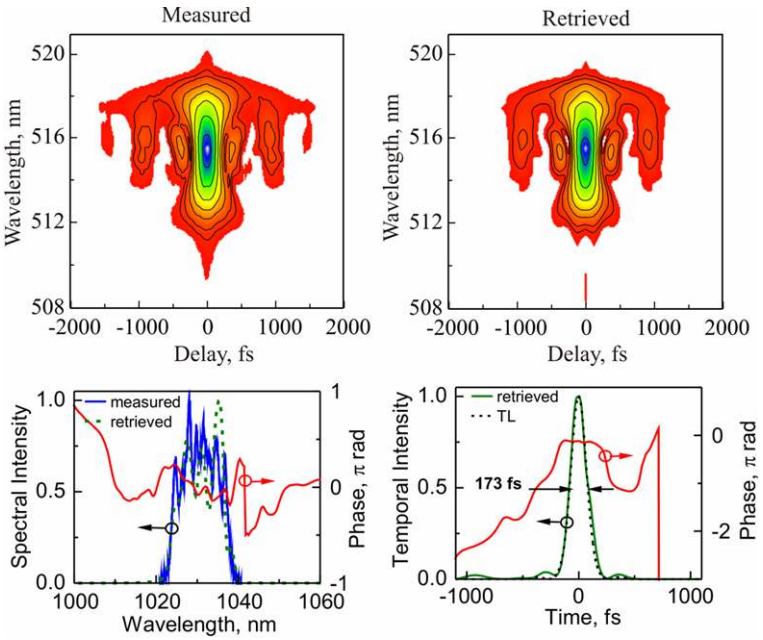

Fig. 14 Recompressed pulse measurement with SHG FROG in the case of the output energy of 1 mJ. TL represents the calculated spectrum-limited pulse

single transmission grating (1700 l/mm, Wasatch Photonics) and a R = −600 mm spherical mirror. Seeded with an unshaped spectrum, the amplifier supports an ∼5-nm bandwidth centered at 1031 nm (dashed curve, Fig. 13). By installing in the Fourier plane of the stretcher an amplitude shaper which modifies the spectrum of the seed light (dotted curve, Fig. 13) we were able to broaden the spectrum of the CRA output to 12 nm FWHM (solid curve, Fig. 13). The spectral pre-shaping introduced an added 60% loss of the seed power. Most of the spectral broadening occurs on the blue side because of a higher gain attained with the cryogenic cooling, which also suppress the GSA.

The amplified pulses were recompressed with a grating compressor based on a single transmission grating (1700 l/mm, Wasatch Photonics). The footprint of the folded compressor is merely 200 mm. The results of pulse characterization with SHG FROG are presented in Fig. 14 and reveal a 173-fs pulse duration, whereas the calculated spectrum-limited pulse duration is ∼165 fs. Such a high level of the compression is achieved with the help of a piezoelectric deformable mirror (Flexible Optical B.V.), installed in the stretcher, which allows careful higher-order dispersion control. Note that special care was taken to maximize the intracavity beam size at highly nonlinear CRA elements (e.g. a 30-mm-long BBO Pockels cell) to keep the level of the overall B-integral of the system low. As evidenced by SHG FROG measurements of the output pulses at different levels of amplification (up to 2.5 mJ of the output energy) for a fixed number of cavity roundtrips, the pulse compressibility is not noticeably affected at high output energies, implying that the nonlinear phase is well under control.

4 Conclusions

The novel Yb host, CaF_2 codoped with Na^+ crystal despite being a low gain cross-section material, presents considerable interest for cw-pumped CRA of multi-mJ ∼200-fs pulses with repetition rates around 1 kHz at cryogenic temperatures. The cooling of the crystal to cryogenic temperatures leads to the disappearance of GSA in the spectral region above 1000 nm and to a substantial increase of the emission and absorption cross-sections, providing the potential for a high-efficiency pumping and energy extraction from the amplifier crystal. The advantages of applying the cryogenic scheme to Na- and Yb-codoped crystals, presented in this paper, make it possible to use conventional laser-diode stacks to pump these crystals at the quantum defect level reduced to about 5%. The pump diodes do not require wavelength stabilization despite the drastic narrowing of absorption linewidths at cryogenic temperatures. In addition, we show that polarization combining may be efficiently utilized for this isotropic crystal to further increase the pumping efficiency without perturbing the emission of the laser diode by a counter-propagating residual pump beam. Furthermore, the Na codoping stimulates the broadening of the absorption on the blue wing of the ZPL which, in comparison with the identical pumping conditions for Yb:CaF_2, permits us to attain a higher population inversion in a Na-containing crystal without running into a problem with parasitic emission losses. Nevertheless, high levels of Na codoping are shown to decrease the emission cross-section, which points out the necessity to choose the Na concentration very carefully.

In the case of the 2%Yb^{3+}-crystal, we have configured the crystal in the regenerative amplifier to have a small sig-

nal single-pass gain of ∼1.33, which is fully sufficient for regenerative amplification despite a heavy spectral modulation induced in the center of the seed spectrum. Considering the development prospects for this cryogenic Yb, Na:CaF_2 technology beyond the first-stage power amplifier, one should attain a significantly higher single-pass gain for a second-stage booster, which would most likely have a multipass amplifier configuration. This can be achieved by employing, e.g., side pumping of the crystals with a 3–4-times higher Yb doping level. A higher Yb^{3+} concentration would be needed, on the one hand, to maintain reasonably high single-pass absorption for pumping the crystal through its "thin" side and, on the other hand, to avoid running into a sizable ground-state population depletion, as was shown in the case of $\beta \approx 0.5$ in Sect. 3.2. Unlike in the three-level room temperature Yb lasers, in the cryogenic (quasi-four-level) version there is no danger of running into the GSA problem while working at a low value of β. On the contrary, leaving a significant pool of unexcited Yb^{3+} ions in the ground state helps avoiding absorption saturation and, as a consequence, permits one to reach a higher single-pass gain for a given pump rate.

As shown in this work, 3-mJ pulses at a 1-kHz repetition rate are straightforwardly available from a single-stage amplifier. Amplification beyond 3 mJ is feasible by improving the quality of surface polishing and AR coatings, as well as by optimizing the CRA cavity. Spectral shaping of the spectral amplitude of the seed and active control of the higher-order phase appear to be crucial for obtaining close to transform limited sub-200 fs pulses at a multi-mJ energy level. Further energy scaling toward tens of mJ appears feasible by designing a cw-diode laser transversally pumped cryogenically cooled Yb^{3+}, Na^{+}:CaF_2 multipass amplifier with an increased Yb^{3+} doping.

Acknowledgement This work is supported by the Austrian Science Fund (FWF), grants U33-N16 and F1619-N08.

References

1. T. Brabec, F. Krausz, Rev. Mod. Phys. **72**, 545 (2000)
2. A. Dubietis, R. Butkus, A.P. Piskarskas, IEEE J. Sel. Top. Quantum Electron. **12**, 163 (2006)
3. G.A. Mourou, T. Tajima, S.V. Bulanov, Rev. Mod. Phys. **78**, 309 (2006)
4. A. Jouini, A. Brenier, Y. Guyot, G. Boulon, H. Sato, A. Yoshikawa, K. Fukuda, T. Fukuda, Cryst. Growth Des. **8**, 808 (2008)
5. A. Lucca, G. Debourg, M. Jacquemet, F. Druon, F. Balembois, P. Georges, P. Camy, J.L. Doualan, R. Moncorge, Opt. Lett. **29**, 2767 (2004)
6. J. Du, X. Liang, Y. Wang, L. Su, W. Feng, E. Dai, Z. Xu, J. Xu, Opt. Express **13**, 7970 (2005)
7. F. Druon, F. Balembois, P. Georges, Opt. Express **12**, 5005 (2004)
8. L. Su, J. Xu, Y. Xue, C. Wang, L. Chai, X. Xu, G. Zhao, Opt. Express **13**, 5635 (2005)
9. S. Biswal, J. Nees, A. Nishimura, H. Takuma, G. Mourou, Opt. Commun. **160**, 92 (1999)
10. H. Liu, J. Nees, G. Mourou, S. Biswal, G.J. Spühler, U. Keller, N.V. Kuleshov, Opt. Commun. **203**, 315 (2002)
11. A. Beyertt, D. Nickel, A. Giesen, Appl. Phys. B **80**, 655 (2005)
12. P. Raybaut, F. Balembois, F. Druon, P. Georges, IEEE J. Quantum Electron. **41**, 415 (2005)
13. M. Siebold, M. Hornung, S. Bock, J. Hein, M.C. Kaluza, J. Wemans, R. Uecker, Appl. Phys. B **89**, 543 (2007)
14. M. Siebold, M. Hornung, R. Boedefeld, S. Podleska, S. Klingebiel, C. Wandt, F. Krausz, S. Karsch, R. Uecker, A. Jochmann, J. Hein, M.C. Kaluza, Opt. Lett. **33**, 2770 (2008)
15. W.F. Krupke, IEEE J. Sel. Top. Quantum Electron. **6**, 1287 (2000)
16. T.Y. Fan, A. Sanchez, IEEE J. Quantum Electron. **26**, 311 (1990)
17. P. Sorokin, M. Stevenson, Phys. Rev. Lett. **5**, 557 (1960)
18. G. Boyd, R. Collins, S. Porto, A. Yariv, W. Hargreaves, Phys. Rev. Lett. **8**, 269 (1962)
19. R.J. Keyes, T.M. Quist, Appl. Phys. Lett. **4**, 59 (1964)
20. M.J. Weber, *Handbook of Optical Materials* (CRC Press, Boca Raton, 2003)
21. L. Su, J. Xu, H. Li, L. Wen, Y. Zhu, Z. Zhao, Y. Dong, G. Zhou, J. Si, Chem. Phys. Lett. **406**, 254 (2005)
22. L. Su, J. Xun, H. Li, W. Yang, Z. Zhao, J. Si, Y. Dong, G. Zhou, Opt. Lett. **30**, 1003 (2005)
23. D.J. Ripin, J.R. Ochoa, R.L. Aggarwal, T.-Y. Fan, IEEE J. Quantum Electron. **41**, 1274 (2005)
24. S. Tokita, J. Kawanaka, Y. Izawa, M. Fujita, T. Kawashima, Opt. Express **15**, 3955 (2007)
25. J. Kawanaka, K. Yamakawa, H. Nishioka, K. Ueda, Opt. Lett. **28**, 2121 (2003)
26. K. Ogawa, Y. Akahane, M. Aoyama, K. Tsuji, S. Tokita, J. Kawanaka, H. Nishioka, K. Yamakawa, Opt. Express **15**, 8598 (2007)
27. D.C. Brown, IEEE J. Quantum Electron. **34**, 2393 (1998)
28. D.C. Brown, IEEE J. Sel. Top. Quantum Electron. **11**, 587 (2005)
29. G. Boulon, in *Advances in Spectroscopy for Lasers and Sensing*, ed. by B. Bartolo, O. Forte (Springer, Dordrecht, 2006), pp. 83–102
30. M. Ito, C. Goutaudier, Y. Guyot, K. Lebbou, T. Fukuda, G. Boulon, J. Phys., Condens. Matter **16**, 1501 (2004)
31. V. Petit, P. Camy, J.-L. Doualan, X. Portier, R. Moncorge, Phys. Rev. B **78**, 085131 (2008)
32. P.-H. Haumesser, R. Gaume, B. Viana, D. Vivien, J. Opt. Soc. Am. B **19**, 2365 (2002)
33. J. Kawanaka, K. Yamakawa, H. Nishioka, K. Ueda, Opt. Express **10**, 455 (2002)
34. A.E. Siegman, *Lasers* (University Science Books, 1986)
35. W. Köchner, Solid-state laser engineering, 6th revised and updated ed: Springer Science+Business Media, Inc., 2006
36. J.A. Caird, S.A. Payne, P.R. Staver, A.J. Ramponi, L.L. Chase, W.F. Krupke, IEEE J. Quantum Electron. **24**, 1077 (1988)